AIAA JOURNAL
Vol. 61, No. 4, April 2023

Modulation and Annihilation of Aeroelastic Limit-Cycle Oscillations Using a Variable-Frequency Disturbance Generator

Michael T. Hughes,* Ashok Gopalarathnam,† and Matthew Bryant‡
North Carolina State University, Raleigh, North Carolina 27695

https://doi.org/10.2514/1.J062295

Nonlinear aeroelastic limit-cycle oscillations (LCOs) have become an area of interest due to both detrimental effects on flying vehicles and use in renewable energy harvesting. Initial studies on the interaction between aeroelastic systems and incoming flow disturbances have shown that disturbances can have significant effects on LCO amplitude, with some cases resulting in spontaneous annihilation of the LCO. This paper explores this interaction through wind-tunnel experiments using a variable-frequency disturbance generator to produce flow disturbances at frequencies near the inherent LCO frequency of an aeroelastic system with pitching and heaving degrees of freedom. The results show that incoming disturbances produced at frequencies approaching the LCO frequency from below produce a cyclic growth-decay in LCO amplitude that resembles interference between multiple sine waves with slightly varying frequencies. An aeroelastic inverse technique is applied to the results to study the transfer of energy between the pitching and heaving degrees of freedom as well as the aerodynamic power moving into and out of the system. Finally, the growth-decay cycles are shown to both excite LCOs in an initially stationary wing and annihilate preexisting LCOs in the same wing by appropriately timing the initiation and termination of disturbance generator motion.

Nomenclature

b	=	airfoil semichord length, m
C_L	=	lift coefficient
C_M	=	aerodynamic moment coefficient
c	=	airfoil chord length, m
c_h	=	damping for heave degree of freedom, N · s/m
c_θ	=	damping for pitch degree of freedom, N · m · s/rad
dt	=	differential time
$E_{x_\theta,h}$	=	coupling energy transfer from the pitch to heave degree of freedom, J
$E_{x_\theta,\theta}$	=	coupling energy transfer from the heave to pitch degree of freedom, J
F_f	=	friction force in the heave degree of freedom, N
f_{LCO}	=	inherent limit-cycle oscillation frequency, Hz
f_{osc}	=	variable-frequency disturbance generator oscillation frequency, Hz
h	=	heave displacement, m
I_θ	=	pitching inertia about the midchord of the aeroelastic wing apparatus, kg · m^2
k_h	=	spring stiffness for heave degree of freedom, N/m
k_θ	=	spring stiffness for pitch degree of freedom, N · m/rad
l_s	=	span length, m
M_f	=	moment due to friction for pitch degree of freedom, N · m
m_{total}	=	total moving mass of aeroelastic wing apparatus, kg
m_w	=	mass of all rotating components in aeroelastic wing apparatus, kg
$< q(t) >$	=	phase-averaged dynamic pressure, Pa
q_∞	=	freestream dynamic pressure, Pa
T	=	period of a single oscillation in the aeroelastic wing apparatus, s
T_c	=	period of a growth-decay cycle, s
t	=	instantaneous time, s
U_∞	=	freestream velocity, m/s
x_θ	=	nondimensional distance (by semichord) from pitching axis to rotational center of mass
θ	=	pitch-oscillation angle, rad
ρ	=	density, kg/m^3

Received 29 July 2022; revision received 7 November 2022; accepted for publication 4 January 2023; published online 7 February 2023.

*Associate Professor, Department of Mechanical and Aerospace Engineering. Member AIAA.
†Professor, Department of Mechanical and Aerospace Engineering. Member AIAA.
‡Graduate Research Assistant, Department of Mechanical and Aerospace Engineering. Student Member AIAA.

I. Introduction

THE study of aeroelasticity and its effects, both positive and negative, is as old as aviation itself. The Wright brothers' use of wing warping to control their aircraft [1] or the failure of Langley's tandem monoplane due to aeroelastic divergence just nine days before the Wright brothers' historic flight at Kitty Hawk [2] shows that even early aviation pioneers were presented with this issue. Instances of in-flight flutter began to occur more frequently as the aviation industry matured; and in 1935, Theodorsen published his landmark study on aeroelastic flutter [3]. Aeroelasticity research today includes a variety of topics including small-scale power generation [4,5], practical solutions for thin-wing aircraft experiencing limit-cycle oscillations (LCOs) [6,7], aeroelastic flutter in the transonic region [8], on-wing flutter mitigation [9–11], and analytical prediction models for nonlinear aeroelasticity [12–14]. The majority of these modern research applications depends on nonlinear flutter analysis and often requires more robust prediction models coupled with computational or experimental validation of such models.

Recent studies concerning nonlinear aeroelastic systems have focused on limit-cycle oscillations in which the system, such as a slender wing, experiences a bounded-amplitude cyclic motion in the pitch and/or heave degrees of freedom. This phenomenon can lead to structural failure of the system, loss of aerodynamic performance, and a reduction in the lifespan of a system due to additional fatigue stress [15]. For most cases involving nonlinear systems, LCOs arise once the system exceeds its flutter speed, which is determined through analysis or experiment. However, in some cases, LCOs can be excited below the flutter speed with a large enough deflection [16]. These deflections exhibit instabilities that result in oscillations that grow in amplitude until they reach a stable bound for a given airspeed. This case represents a subcritical Hopf bifurcation and was referred to as "bad LCO" by Dowell et al. [16]. LCOs arising from subcritical Hopf bifurcations can be problematic for aeroelastic systems that are initially stable but experience changing conditions such as the introduction of external stores on a thin-wing jet fighter or the presence of incoming flow disturbances from an external source.

The interactions between impinging flow disturbances and aeroelastic systems, especially systems subject to LCOs, have recently become an area of interest and are not fully understood. However, flapping wings in the presence of incoming flow disturbances have been the topic of several studies and bear some similarities to aeroelastic systems. Lua et al. [17] showed that vortices interacting with a heaving wing can be categorized as either lift producing or lift reducing, depending on whether the wing encounters a pair of counter-rotating vortices or a single vortex. In a second study, Lua et al. [18] showed that adding a pitching motion to the flapping wing also affected the lift enhancement produced by impinging vortices. Additionally, Kinsey and Dumas [19] showed that a leading-edge vortex that is shed in time with the pitching and heaving motion of an oscillating airfoil can improve its propulsive efficiency. Because aeroelastic systems experiencing LCOs also experience unsteady flow due to pitch–heave oscillations, the results of these studies may also have implications for the interactions between aeroelastic systems and impinging vortices. Recently, Okshai et al. [20] examined an aeroelastic energy-harvesting device in a periodic wake produced by an oscillating foil placed upstream. Their results showed that the downstream aeroelastic device experienced amplitude modulation when exposed to incoming flow disturbances with a high degree of sensitivity to the frequency of the flow disturbances.

Previous work done in the Intelligent Systems and Structures Research Laboratory at North Carolina State University (NCSU) has focused on studying the interactions between aeroelastic systems and incoming flow disturbances as well as the impact they have on the aeroelastic properties of an elastically supported wing section. Gianikos et al. [21] placed a static, rectangular bluff body upstream of an aeroelastic wing to observe the effects of vortices produced by the bluff body on the downstream wing. Their results showed that the impinging vortices, produced at a rate approximately three times the oscillation frequency of the downstream wing, caused significant modulation in the oscillation amplitude of the wing in both the pitch and heave degrees of freedom. Using the same bluff body and aeroelastic wing, but with a different center of mass location, Kirschmeier et al. [22] observed passive LCO annihilation, in which the downstream wing spontaneously returned to a stable, equilibrium position from LCO. LCO annihilation in the presence of the static bluff body, for which the rate of vortex generation is proportional to the freestream velocity, led to the desire for a system in which the rate of vortex generation could be varied on demand independently of the flow conditions. Such a system would allow study of the interactions between an aeroelastic wing and incoming flow disturbances at a wide range of flow conditions and vortex generation frequencies. Research done by Rockwood and Medina [23] and Chatterjee et al. [24] demonstrated that a pitch-oscillating cylinder with an attached splitter plate is able to produce a "locked-in" von Kármán, vortex street with vortices being produced at the rate of oscillation.

This paper demonstrates the unique interactions between an aeroelastic wing and incoming vortices produced by a variable-frequency disturbance generator (VFDG). At disturbance generator frequencies very near, but just below, the inherent LCO frequency of the wing, the impinging vortices produce a wing response dominated by large cyclic fluctuations in the wing oscillation amplitude in both pitch and heave. Using this behavior, LCOs can be both excited and annihilated in the aeroelastic wing. Data analysis of the wing response is performed using signal processing techniques and an aeroelastic inverse method developed by Kirschmeier et al. [25]. The information gathered from the analysis provides insight into the fundamental physics present during the interaction between the wing and incoming vortices and may prove useful in developing future LCO mitigation strategies. The remainder of this paper will discuss the testing apparatus and strategies in Sec. II, initial results from the experimental campaign in Sec. III, and further analysis on the most interesting data as well as practical applications of the results in Sec. IV. Section V offers suggestions for future work moving forward. Finally, Sec. VI will present a summary of the work done in this report.

II. Materials and Methods

A. Aeroelastic Wing Apparatus

The aeroelastic wing apparatus used for this work is summarized here and described in detail by Gianikos et al. [21] and Kirschmeier et al. [22]. A decambered, symmetric version of an SD 7003 airfoil with a chord length of 0.15 m and an aspect ratio of four was chosen for the aeroelastic wing. The wing was constructed from Acrylonitrile butadiene styrene (ABS) plastic using three three-dimensionally printed sections with two 3.175 mm (1/8 in.) aluminum spars running the length of the wing. The exterior surface of the wing was primed and sanded to create a smooth finish on the wing's surface. Elliptical endplates extending one chord length fore and aft of the wing were added to both ends of the wing to emulate two-dimensional flow based on the work of Visbal and Garmann [26]. A rail and carriage system, shown in Fig. 1, was designed to accommodate degrees of freedom (DOFs) in both pitching and heaving. The wing was attached to the carriage system, which translated in the cross-stream direction along linear rails mounted above and below the wind-tunnel test section, providing the heave degree of freedom. Additionally, the carriages included radial ball bearings, which allowed the wing to rotate about its pitching axis. For the work done in this paper, the pitching axis of the wing is located at the midchord. Linear extension springs are used to provide the elastic restoring force for both the heave and pitch degrees of freedom. For the heave DOFs, the springs are mounted parallel to the linear rail and attached between a rigid mount on either side of the carriage. Four springs are used for the pitch DOFs with two mounted on each carriage, allowing them to translate along with the wing. The springs are attached to the rotation axis of the wing using a pulley and cable. Although the pitch stiffness can exhibit nonlinearity due to the springs on one side of the pulley becoming slack at sufficiently large angles [21], the pitch stiffness remains in the linear range for all the experiments reported in this study. A summary of the mass, stiffness, geometry, and inertia properties of the apparatus is shown in Table 1. The effective stiffness listed in the table denotes the combined stiffness properties acting on the wing from both upper and lower carriages. An in-depth discussion of the stiffness characteristics of the system can be found in the works of Gianikos et al. [21] and Kirschmeier et al. [22].

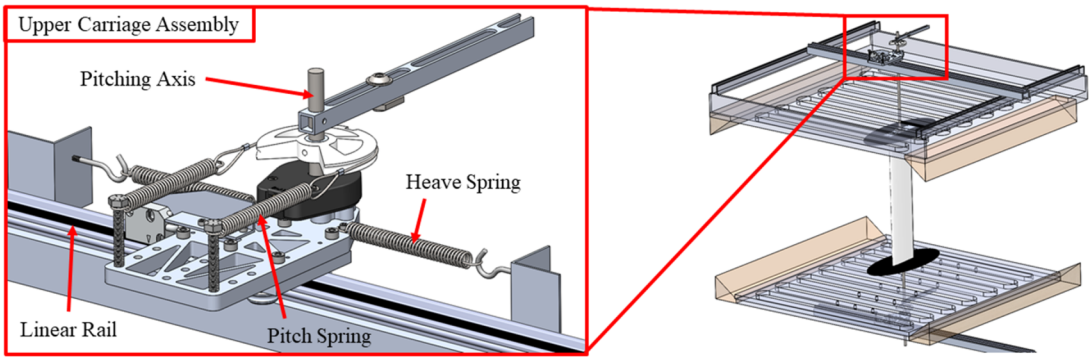

Fig. 1 CAD mockup of the aeroelastic wing apparatus highlighting the upper carriage assembly.

Table 1 Mass, inertia, and stiffness properties of aeroelastic wing apparatus

Parameter	Description	Value
m_{total}	Total mass of all moving parts	3.268 kg
m_{ω}	Mass of all rotating parts	1.609 kg
I_{θ}	Pitching inertia about midchord	5.77e-03 kg · m^2
c	Chord length	0.15 m
l_s	Span length	0.6 m
x_{θ}	Nondimensional distance from pitch axis to center of mass	7.82e-2
k_h	Effective heave stiffness	2.17e-3 N/m
k_{θ}	Effective pitch stiffness in linear range	3.59 N · m/rad

B. Variable-Frequency Disturbance Generator

Following the observation of LCO annihilation in the aeroelastic wing due to interactions with the vortical wake of a static rectangular bluff body by Kirschmeier et al. [22], the development of a variable-frequency disturbance generator was motivated by the need for greater control over the vortex shedding frequency. The static bluff body used in previous work was sized to shed vortices at a rate near the third harmonic of the wing's LCO frequency for flow speeds ranging from 9 to 12 m/s. For static bluff bodies, the vortex shedding frequency is tied to the freestream velocity. However, a VFDG allows for multiple shedding frequencies while maintaining a constant flow rate. Experiments performed by Rockwood and Medina [23] compared a stationary cylinder, an oscillating cylinder, and an oscillating cylinder with an attached splitter plate at the trailing edge. Although their results showed that both oscillating cylinders could shed vortices at a rate equal to their oscillation frequency, the inclusion of the attached splitter plate produced a more well-defined wake at a wider range of oscillation frequencies. As a result, the cylinder with an attached splitter plate configuration was chosen for the VFDG.

The materials selected for the disturbance generator were chosen to minimize mass and inertia, thereby reducing the necessary electrical power needed to drive the oscillation at the required frequencies. The primary cylinder was constructed from a 10.48-cm-diameter (4.125-in.-diameter) braided, carbon fiber tube with a 45 deg fiber orientation produced by DragonPlate™ (Elbridge, New York). The attached splitter plate extended away from the axis of rotation on only one side of the cylinder, thereby constituting a significant portion of the inertia for the system. A 1.59-mm-thick (1/16-in.-thick) carbon fiber and birch wood composite plate produced by DragonPlatewas selected as the splitter plate material to reduce inertia while maintaining stiffness. Additional structural components were constructed from aluminum, and stainless-steel fasteners were used throughout the structure. As shown in Fig. 2, the central mounting shafts were split into two sections so that the attached splitter plate could extend across the full diameter of the primary cylinder to ensure a rigid mount and avoid "flapping" during oscillation. Table 2 lists the complete mass and inertia properties of the variable-frequency disturbance generator and its component subassemblies.

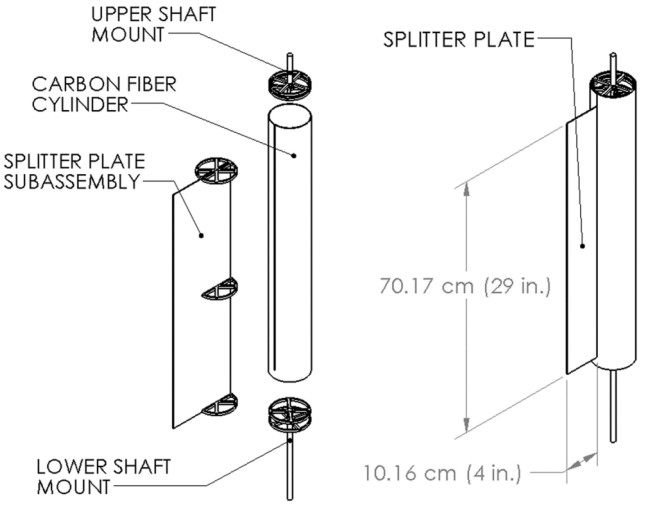

Fig. 2 Variable-frequency disturbance generator diagram showing construction process and final assembly.

Table 2 Estimated mass and inertia properties of variable-frequency disturbance generator and subassemblies

Subassembly	Mass, g	Inertia about axis of rotation, g · m^2	Contribution to total inertia, %
Cylinder	594.2	1.582	41
Splitter plate	432.6	1.889	49
Shaft assemblies	269.5	0.225	6
Fasteners	63.3	0.153	4
Total	1359.6	3.849	— —

C. Electrical Systems and Data Acquisition

Oscillation of the VFDG was driven by a SureServo SVL-210b produced by AutomationDirect (Cumming, Georgia) with a maximum continuous torque of 3.3 N · m and a maximum instantaneous torque of 9.9 N · m. For the tests outlined in this paper, oscillation followed a sinusoidal trajectory supplied by a Keysight (Santa Rosa, California) 33500B waveform generator that was fed in as an analog input to a Copley Controls (Canton, Massachusetts) Xenus XTL-230-18 digital servo drive. Although the SureServo motor's built-in encoder was used to track the motor trajectory for control purposes with the Xenus drive, an additional US Digital (Vancouver, Washington) E6-10000 optical encoder was used to track the disturbance generator oscillation angle during testing. Sensors on the downstream wing included two US Digital E6-10000 optical encoders and a Renishaw LM10 (West Dundee, Illinois) magnetic linear encoder. The optical encoders were placed on the upper and lower carriage assemblies for the wing and were averaged to find the real-time pitch angle of the wing. The linear encoder was attached to the lower carriage assembly and used to record the linear heave displacement of the wing in real time. A National Instruments (NI) PXIe-1078 data acquisition system running NI LabVIEW was used to record real-time data during testing. The four encoders were wired into an NI SCB-68A terminal block, and data were acquired at a sampling frequency of approximately 500 Hz. Constant-temperature anemometry (CTA) was performed using a Dantec Dynamics (Skovlunde, Denmark) MiniCTA 54T30 and a 55P11 miniature hot-wire probe oriented straight into the oncoming flow.

D. North Carolina State University Subsonic Wind Tunnel

The NCSU subsonic wind tunnel, located on NCSU's Centennial Campus, is a closed-return wind tunnel with a 0.81 m (32 in.) by 1.14 m (45 in.) by 1.17 m (46 in.) test section. Flow in the tunnel is driven by a variable-pitch fan powered by a three-speed electric motor. The freestream dynamic pressure is controlled by changing the blade pitch at each of the three motor speeds. Turbulence is controlled passively by two fine screens, a high-aspect-ratio honeycomb, and a contraction section upstream of the test section. The maximum dynamic pressure attainable in the test section is 720 Pa (15.0 lb/ft^2), corresponding to a freestream velocity of approximately 40 m/s at nominal temperature and atmospheric pressure.

E. Experimental Procedure

The primary goal of the experiments in this paper was to study the interaction between incoming flow disturbances produced by the VFDG and the aeroelastic wing apparatus. The first series of tests, which were designed to characterize the response of the aeroelastic wing in self-sustaining LCO without any upstream disturbances, were run at prescribed freestream dynamic pressures ranging from 33.5 Pa (0.70 lb/ft^2) to 62.2 Pa (1.30 lb/ft^2) in increments of approximately 4.8 Pa or 0.1 lb/ft^2. LCOs in the wing were excited manually by increasing the pitch angle by hand and releasing the wing. This initial perturbation caused the wing to enter self-sustaining LCO in the same

fashion as described by Gianikos et al. [21] and Kirschmeier et al. [22]. The second series of tests had three main goals: characterize the general response of the aeroelastic wing in the presence of impinging vortices produced by the VDFG at a range of oscillation frequencies; use the VFDG to excite self-sustaining LCOs in the wing that persist after the VFDG oscillations are stopped; and use the VFDG to annihilate preexisting LCOs in the wing, causing it to return to an equilibrium position. For all of these tests, the VFDG was placed upstream of the wing at a distance of eight cylinder diameters measured from the cylinder center to the wing leading edge. The test section dynamic pressure for these tests was set to 47.9 Pa (1.00 $\mathrm{lb/ft^2}$), corresponding to a freestream velocity of 9.25 m/s. An additional series of tests was performed at dynamic pressures of 52.7 Pa (1.10 $\mathrm{lb/ft^2}$), 59.85 Pa (1.25 $\mathrm{lb/ft^2}$), and 71.8 Pa (1.50 $\mathrm{lb/ft^2}$) to determine the sensitivity of the system to differing freestream conditions. The VFDG oscillation amplitude was set to 30 deg with frequencies ranging from 3.5 to 4.5 Hz in increments of 0.1 Hz. In the range from 3.9 to 4.1 Hz, near the expected LCO frequency of 4 Hz, an increment of 0.01 Hz was used. During all tests, the aeroelastic wing apparatus was set up in the format used by Kirschmeier et al. [22]. The VFDG oscillation profile was prescribed as a constant-amplitude sine wave supplied by the Xenus controller and triggered using a custom LabVIEW virtual instrument (VI). The VFDG oscillation angle, wing pitch angle, and wing heave displacement were recorded at time-synchronized instances using the same VI at a rate of approximately 500 Hz. For undisturbed tests, data were recorded for a minimum of 60 s. For tests with the disturbance generator, a minimum "generator-on" time of 30 s was used. When a self-sustaining LCO was successfully excited, data were continually recorded for an additional 60 s minimum and continued until the wing came to rest either through LCO annihilation or by tunnel dynamic pressure reduction.

III. Results

A. LCO Characterization of the Aeroelastic Wing

Before the addition of the VFDG, the response of the aeroelastic wing in the absence of incoming disturbances was examined to provide a baseline for comparison. The same procedure discussed by Gianikos et al. [21] and Kirschmeier et al. [22] was used to excite LCOs in the wing. The wing was manually perturbed beyond a minimum pitch angle of approximately 0.5 rad (≈30 deg) and released: at which point, it began to demonstrate self-sustaining LCOs dominated by stall flutter with the quarter-chord instantaneous angles of attack reaching above 50 deg, as shown in Fig. 3. Figure 3h demonstrates the cyclic nature of the wing response. The instantaneous angle of attack (AOA) was calculated by finding the angle between the resultant velocity vector (freestream velocity plus wing motion) at the wing quarter-chord and the wing chord line at each instance in time. Although there were two sources on nonlinearity for the system (stall flutter and pitch spring slackness), the wing pitch for these experiments did not reach the threshold needed to induce the pitch spring slackness of 1.08 rad (62 deg). Because the wing pitch angle did not go beyond this value during the testing campaign, the source of nonlinearity was limited to the stall flutter. A detailed discussion of the stiffness nonlinearity was presented by Gianikos et al. [21]. LCOs continued indefinitely until the prescribed dynamic pressure was reduced enough to allow the wing to come to rest. In the absence of the disturbance generator, increasing dynamic pressure produced an increase in the amplitude of the wing's pitch angle and heave displacement, as shown in Fig. 4a. It is worth noting that the heave amplitude appears to peak or asymptotically approach a value of $h/c \approx 0.32$, whereas the pitch amplitude continues to increase with dynamic pressure. Alternatively, the frequency response of the wing pitch and wing heave, obtained via fast-Fourier transform (FFT), shows a reduction in the LCO frequency as dynamic pressure is increased, as presented in Fig. 4b.

B. Disturbance Generator Wake Characterization

The wake behind the VFDG was characterized at a dynamic pressure of 47.9 Pa (1.00 $\mathrm{lb/ft^2}$) using hot-wire anemometry at three downstream distances: immediately behind the splitter plate, midway to the wing leading-edge location, and at the location of the wing quarter-chord. The aeroelastic wing apparatus was not installed during the VFDG wake characterization. At each of these downstream locations, the hot-wire probe was traversed horizontally at increments of 0.0625 cylinder diameters (0.635 cm or 0.25 in.) to ± two cylinder diameters (20.3 cm or 8 in.) from the centerline of the wind-tunnel test section, for a total of 195 discrete points. At each point, the VFDG was oscillated for approximately 60 s at 4.00 Hz and the hot-wire voltage recorded simultaneously. The resulting voltage data were converted to dynamic pressure using a calibration file built from dynamic pressures ranging from 4.79 Pa (0.1 $\mathrm{lb/ft^2}$) to 119.70 Pa (2.5 $\mathrm{lb/ft^2}$). Following the experiments, the data were phase averaged using the method described by Hussein and Reynolds [27] with the VFDG oscillation serving as the reference signal. The resulting phase-averaged dynamic pressure can then be plotted as a function of cycle fraction for any given physical point: an example of which is shown in Fig. 5.

Using each of the 195 discrete locations, cross-stream profiles of the dynamic pressure can be assembled for the complete VFDG oscillation cycle, as shown in Fig. 6. The profiles show that the local dynamic pressure is both transiently reduced and increased by the passing vortices. By plotting these profiles as functions of the cycle

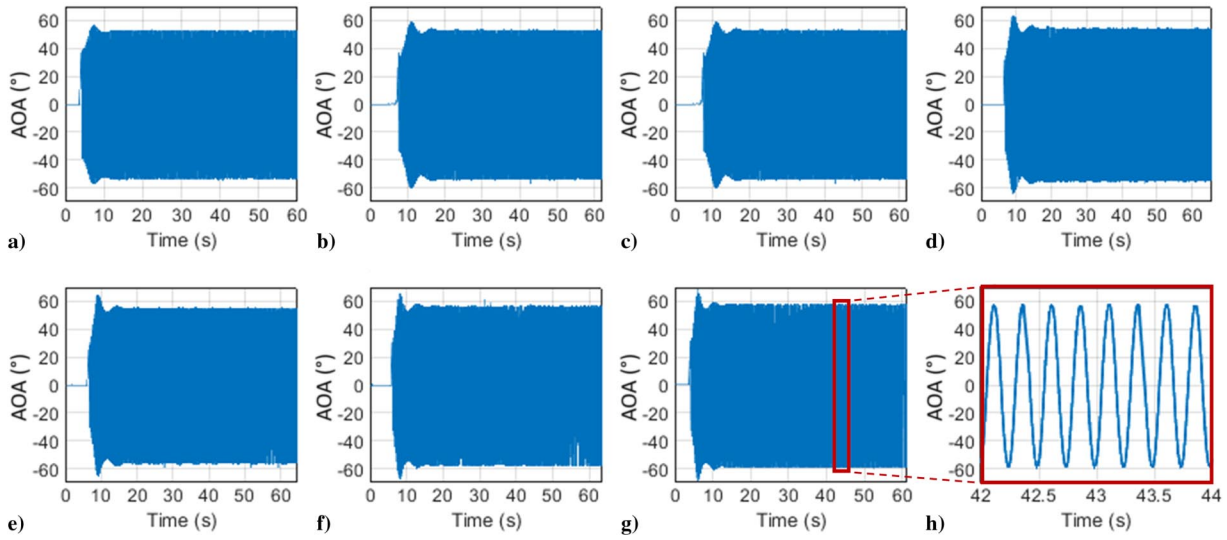

Fig. 3 Instantaneous angle of attack at quarter-chord during LCO for q = a) 33.5 Pa (0.70 $\mathrm{lb/ft^2}$), b) 38.3 Pa (0.80 $\mathrm{lb/ft^2}$), c) 43.1 Pa (0.90 $\mathrm{lb/ft^2}$), d) 47.9 Pa (1.00 $\mathrm{lb/ft^2}$), e) 52.7 Pa (1.10 $\mathrm{lb/ft^2}$), f) 57.5 Pa (1.20 $\mathrm{lb/ft^2}$), and g) 62.2 Pa (1.30 $\mathrm{lb/ft^2}$); and h) zoomed-in section of 62.2 Pa (1.30 $\mathrm{lb/ft^2}$) test to highlight oscillation profile.

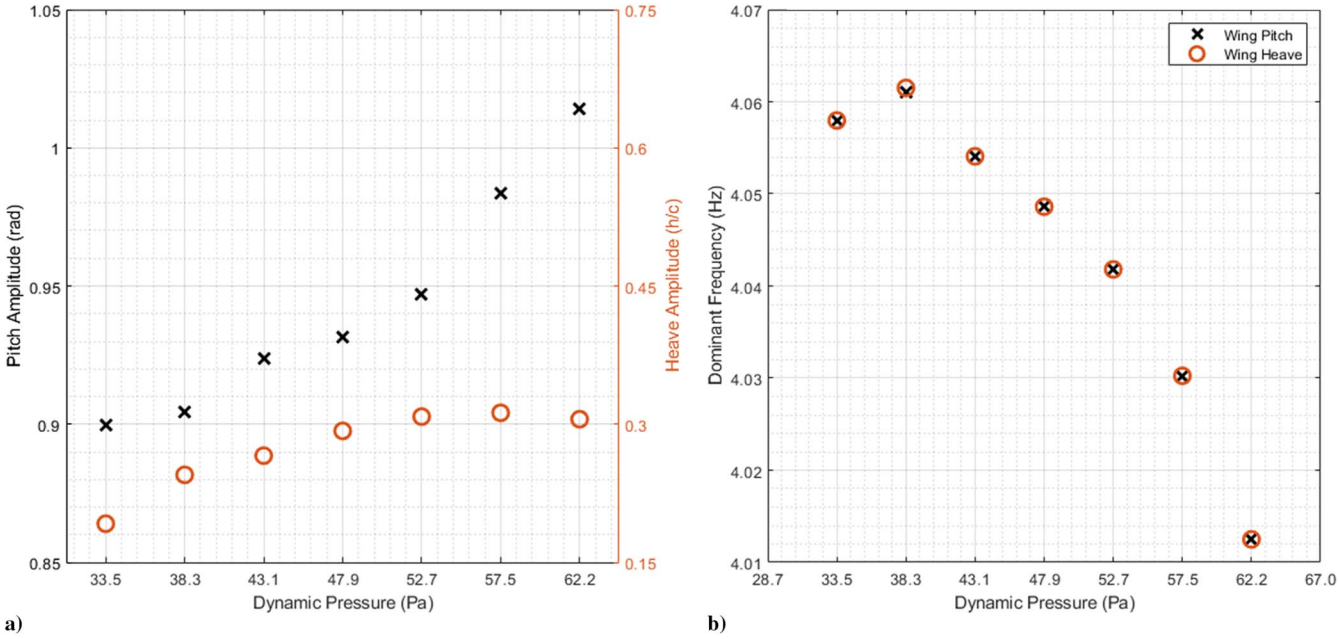

Fig. 4 Results from LCO characterization tests showing a) pitch and heave amplitudes and b) pitch and heave oscillation frequencies as a function of prescribed dynamic pressure.

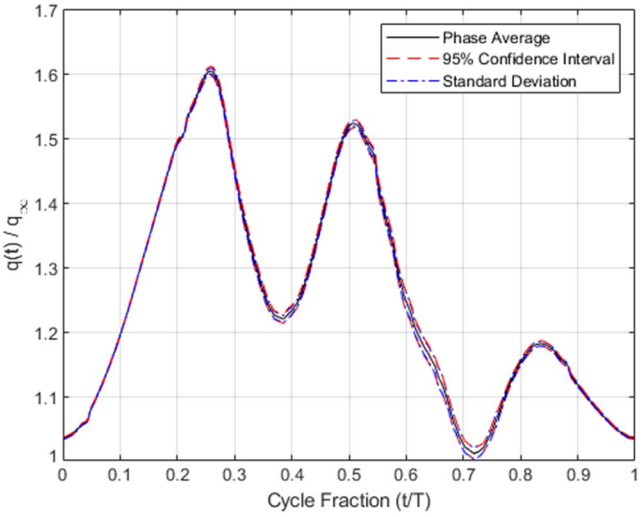

Fig. 5 Phase-averaged dynamic pressure as a function of cycle fraction immediately behind VFDG at a cross-stream location of 1.75 cylinder diameters from test section centerline.

fraction, the shifting deficit/enhancement region can be seen moving to either side of the test section centerline, signifying the shed vortices. Additionally, the reduction/increase of the dynamic pressure, and thereby the strength of the vortices, diminishes as the distance from the VFDG is increased. Near the test section centerline, fast-Fourier transforms performed on the full time history of the dynamic pressure showed dominant frequencies of 8 Hz, corresponding to double the VFDG oscillation frequency. This value is expected if two vortices are shed during each oscillation cycle. Consequently, at locations farthest from the test section centerline, dominant frequencies of 4 Hz were observed. This is likely due to the vortices being shed away from the test section centerline and resulting in locations away from the centerline experiencing effects of only one of the vortices produced during the oscillation cycle.

C. Amplitude Growth and Decay Due to Incoming Flow Disturbances

The results from the test case with dynamic pressure set to 47.9 Pa (1.00 $\mathrm{lb/ft^2}$) and a resulting LCO frequency of approximately 4.05 Hz were used as the baseline for tests with the VFDG placed upstream. The resulting wing response varied as a function of the disturbance generator oscillation frequency. Within the prescribed range of oscillation frequencies (3.5 to 4.5 Hz), five distinct regions of interest can be observed (summarized in Table 3), with each displaying unique characteristics in the wing response.

In the first region of interest with disturbance generator frequencies of 3.5, 3.6, 3.7, and 3.8 Hz, the wing displayed a low-amplitude sinusoidal, buffeting response: examples of which are shown in Figs. 7a and 7b. In each case within this region, the wing pitch and heave oscillation frequencies matched the frequency of the disturbance generator, and the amplitudes remained largely constant for the duration of time it was exposed to incoming vortices. The amplitudes of both pitching and heaving oscillations increased with the disturbance generator frequency. During each test, once the disturbance generator was turned off, the wing returned to an equilibrium position.

The second region of interest includes disturbance generator frequencies ranging from 3.9 to 3.94 Hz in increments of 0.01 Hz. In this region, the wing response displayed significant modulation of the oscillation amplitude in both pitch and heave degrees of freedom just after the disturbance generator began oscillating, as shown in Figs. 7c and 7d. As the vortices began interacting with the aeroelastic wing, it responded with an initial spike in amplitude, followed immediately by a sharp reduction. In some cases, the initial reduction brought the amplitude to near zero in both pitch and heave. Following this initial growth and decay, the pitch and heave amplitudes began to increase again but did not reach the peak amplitude of the first cycle. For tests in this region, this cyclic behavior repeated a few times, with the peak amplitude decreasing on each subsequent cycle until the oscillation amplitude reached an equilibrium state in which there were small fluctuations in the amplitudes of both pitch and heave. As in the first region, once the disturbance generator stopped oscillating, the wing oscillations damped out, and it returned to an equilibrium position.

The third region of interest, with disturbance generator frequencies from 3.95 to 4.04 Hz in 0.01 Hz increments, is characterized by major amplitude modulations, as shown in Figs. 7e–7h. Figure 8 shows a zoomed-in view of the regions of Figs. 7e and 7f to highlight the oscillatory nature of the wing response and is representative of the wing response in other cases as well. These growth-decay cycles resulted from interactions between the incoming vortices and the inherent aeroelastic properties of the wing, namely, the self-sustaining LCO discussed in Sec. III.A in the tests without the disturbance generator. During each test in this range of disturbance generator frequencies, the peak amplitude in the pitch oscillation was greater

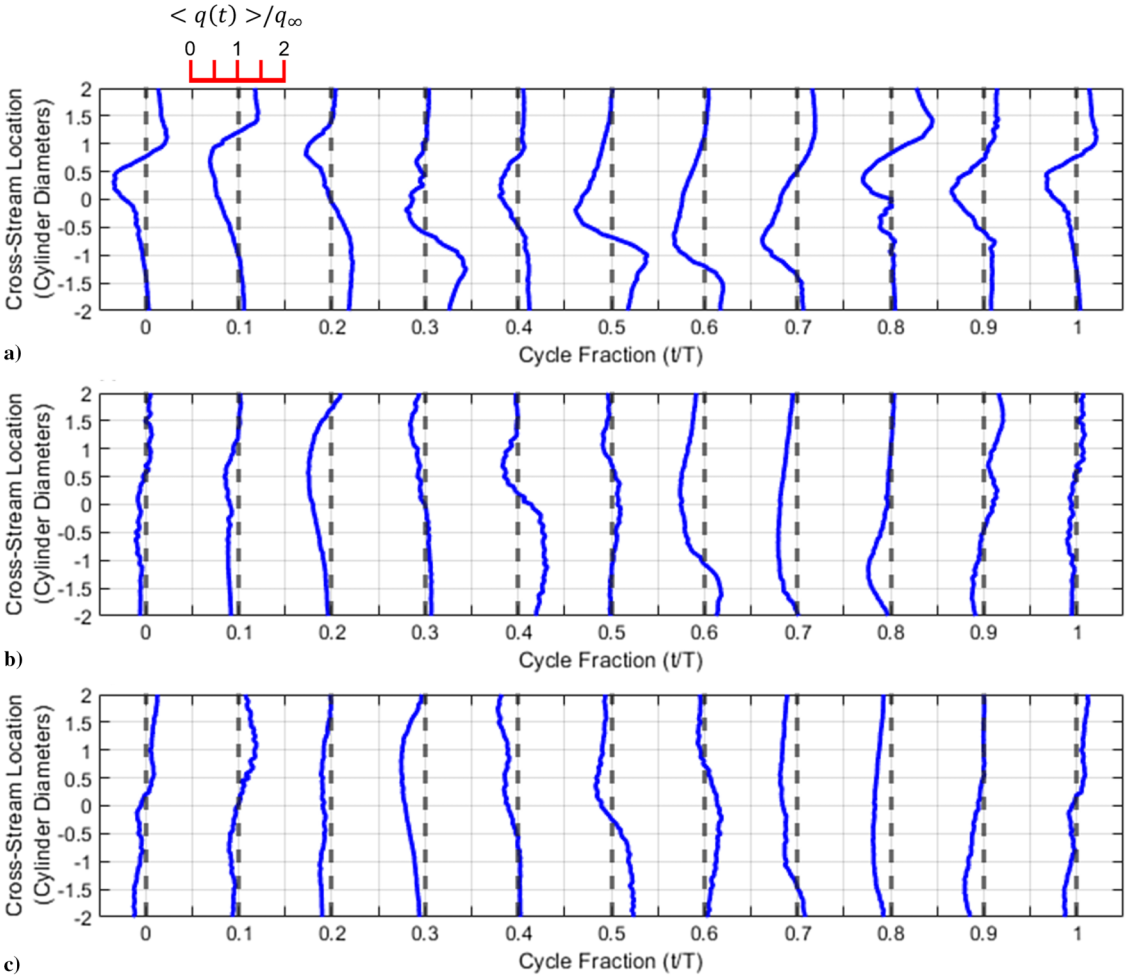

Fig. 6 Cross-stream phase-averaged dynamic pressure profiles as functions of VFDG oscillation cycle fraction at downstream locations a) just behind VFDG, b) midway between VFDG and aeroelastic wing leading-edge location, and c) at location of wing quarter-chord. Phase-averaged dynamic pressure is nondimensionalized by freestream dynamic pressure.

Table 3 Summary of five regions of interest with regard to wing response in presence of varying disturbance generator oscillation frequencies

Region of interest	VFDG oscillation frequency range, Hz	LCO present (Y/N)	Wing response
1	3.50 to 3.80	N	Low-amplitude buffeting
2	3.90 to 3.94	N	Minor amplitude modulation and low-amplitude buffeting
3	3.95 to 4.04	Y	Major amplitude modulation with growth-decay cycles
4	4.05	Y	Self-sustaining LCO without amplitude modulation
5	4.06 to 4.50	N	Low-amplitude buffeting

than the deflection (approximately 30 deg) needed to manually start LCOs for the baseline case. As the disturbance generator oscillation frequency was increased, Fig. 9 shows that there was a corresponding growth in peak amplitude for both pitch and heave oscillations. However, the minimum amplitude in the pitch oscillations shows an inverse relationship with the disturbance generator oscillation frequency. Additionally, at a disturbance generator frequency of 4.04 Hz, the minimum amplitudes for both pitch and heave show a large jump. The pitch and heave oscillations for this case (shown in Figs. 7g and 7h, respectively) displayed a much smaller gap between the maximum and minimum amplitudes during the growth and decay cycles as compared to lower frequencies in this region of interest.

The fourth region of interest only contained one disturbance generator oscillation frequency (4.05 Hz), which corresponded to the dominant frequency of the LCO seen during the undisturbed tests at 47.9 Pa (1.00 $\mathrm{lb/ft^2}$). At this frequency, the wing response, shown in Figs. 7i and 7j, did not display the growth-decay cycles seen in the third region of interest. Apart from an initial period of growth immediately after the disturbance generator began oscillating, the vortices produced by the disturbance generator appeared to have little effect on the wing dynamics. Pitch and heave oscillations showed little to no amplitude modulation, leveling out at the peak values seen in the third region of interest and appearing more similar to undisturbed LCOs seen in prior tests.

The fifth and final region of interest contained disturbance generator oscillation frequencies ranging from 4.06 to 4.5 Hz. Frequencies from 4.06 to 4.1 Hz were varied in 0.01 Hz increments; above 4.1 Hz, the increment was increased to 0.1 Hz. It was observed that the wing response was not symmetric about the inherent LCO frequency of 4.05 Hz. Unlike the third region of interest, the wing behavior in this region shared more traits with the first region. The wing pitch and heave experienced an initial spike in amplitude as the disturbance generator began oscillating (as seen in Figs. 7k and 7l); but, this was immediately damped out, and the wing settled into a low-amplitude oscillation in both degrees of freedom that continued until the disturbance generator oscillations were stopped. As the disturbance generator frequency was further increased, the amplitudes of the pitch and heave oscillations after the initial spike continued to decrease.

D. Sensitivity to Differing Flow Conditions

Following the primary series of tests run at a constant dynamic pressure of 47.9 Pa (1.00 $\mathrm{lb/ft^2}$), an additional series of tests was run

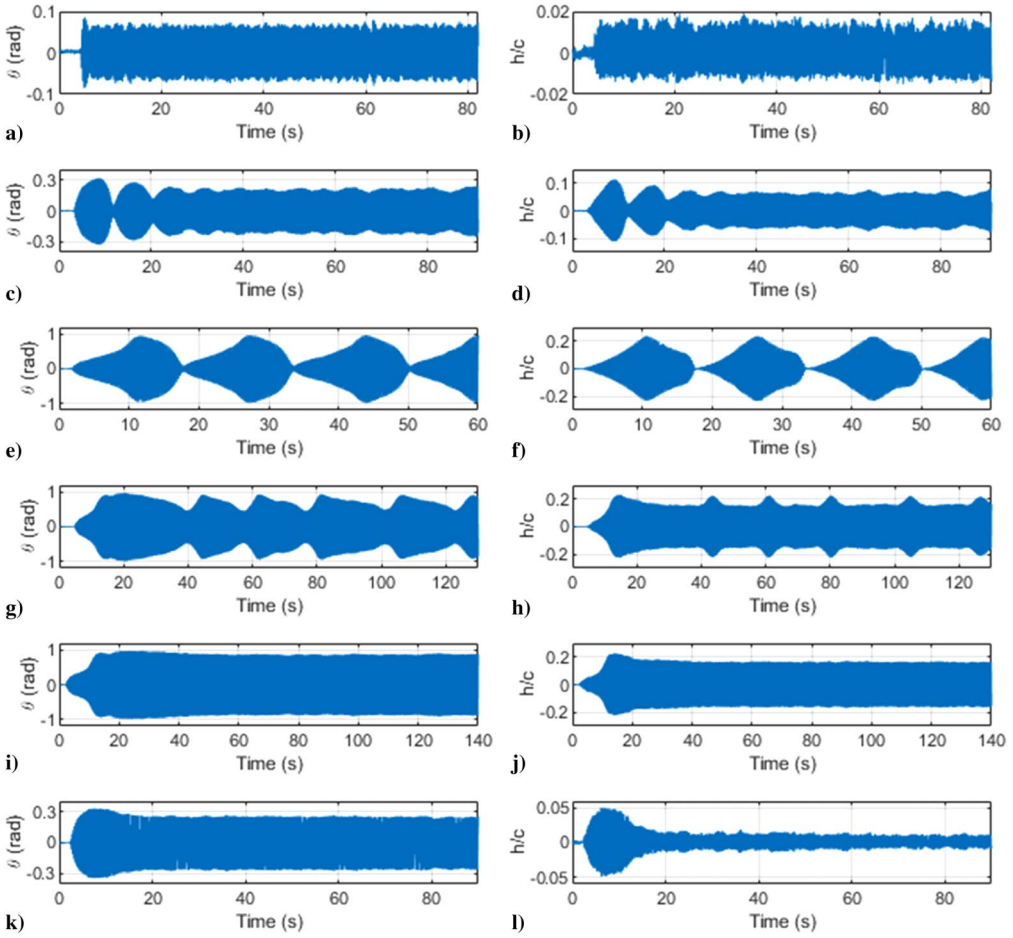

Fig. 7 Wing response examples for five regions of interest (with two examples for third region) with pitch response in left column and heave response in right column. Varied timescales are shown to ensure complete visualization of growth-decay behavior. For each test, dynamic pressure was set to 47.9 Pa (1.00 lb/ft^2).

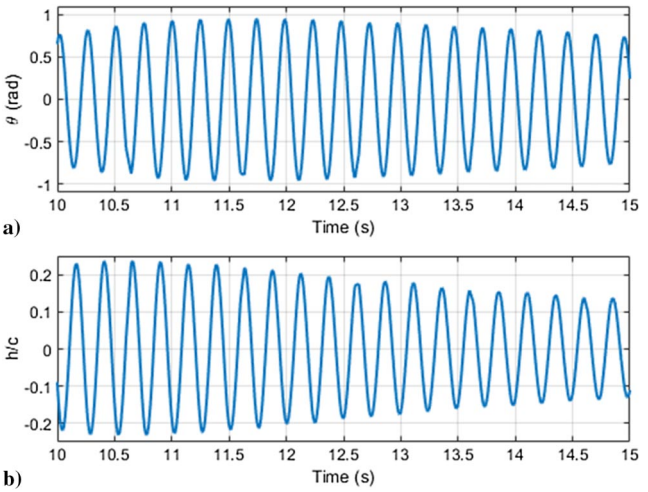

Fig. 8 Zoomed-in regions of time histories of wing a) pitch and b) heave when VFDG oscillation frequency set to 4.0 Hz.

with differing freestream dynamic pressures. The focus for this series of tests was to determine if the cyclic growth and decay leading to self-sustaining LCOs, labeled as the third region of interest in Sec. III.C, would be observed with differing flow conditions and, if so, how the change in freestream dynamic pressure affected the wing response. New dynamic pressures of 52.7 Pa (1.10 lb/ft^2), 59.85 Pa (1.25 lb/ft^2), and 71.8 Pa (1.50 lb/ft^2) were chosen. Due to spring fatigue concerns, the pitch and heave springs attached to the aeroelastic wing apparatus were replaced before these tests. The resulting minor changes to the inherent LCO frequencies were attributed to manufacturing tolerances in the pitch and heave springs.

At each of the three new flow conditions, the cyclic growth and decay found in region 3 was observed (as shown in Fig. 10) but at increasingly lower VFDG oscillation frequencies as compared to the inherent LCO frequency (as seen in Table 4). For dynamic pressures of 52.7 Pa (1.10 lb/ft^2) and 59.85 Pa (1.25 lb/ft^2), the wing response in pitch and heave maintained strong similarities to the 47.9 Pa (1.00 lb/ft^2) results. However, at 71.8 Pa (1.50 lb/ft^2), the wing transitioned to a second growth and decay cycle pattern after the initial response. This new behavior was marked by increased minimum and maximum amplitudes and reduced time between growth-decay cycles. It should be noted that even with the increased amplitude, the wing pitch did not breach the pitch spring slack threshold of 1.08 rad (62 deg).

IV. Analysis and Discussion

A. Applying an Aeroelastic Inverse Method

In an effort to gain further understanding of the underlying physics present during the interactions between the VFDG and the aeroelastic wing, the aeroelastic inverse method derived by Kirschmeier et al. [25] was applied to the results of the 47.9 Pa (1.00 lb/ft^2) test cases. This method was developed to examine the instantaneous aerodynamic forces and moments acting on an aeroelastic wing experiencing high-amplitude pitching and heaving motion. This is accomplished by inverting the equations of motion for the system in order to solve for the lift and moment coefficients of the aeroelastic system as functions of time, as seen in Eqs. (1) and (2),

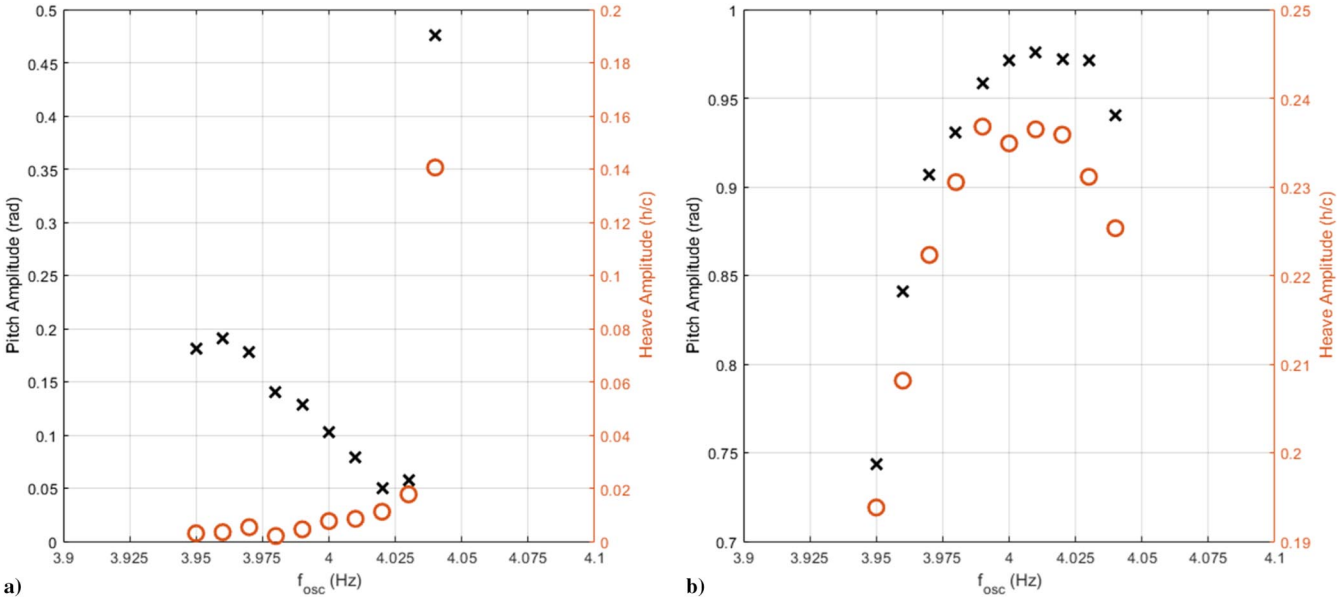

Fig. 9 Pitch and heave amplitudes as functions of disturbance generator oscillation frequency showing a) mean minimum amplitude and b) mean maximum amplitude.

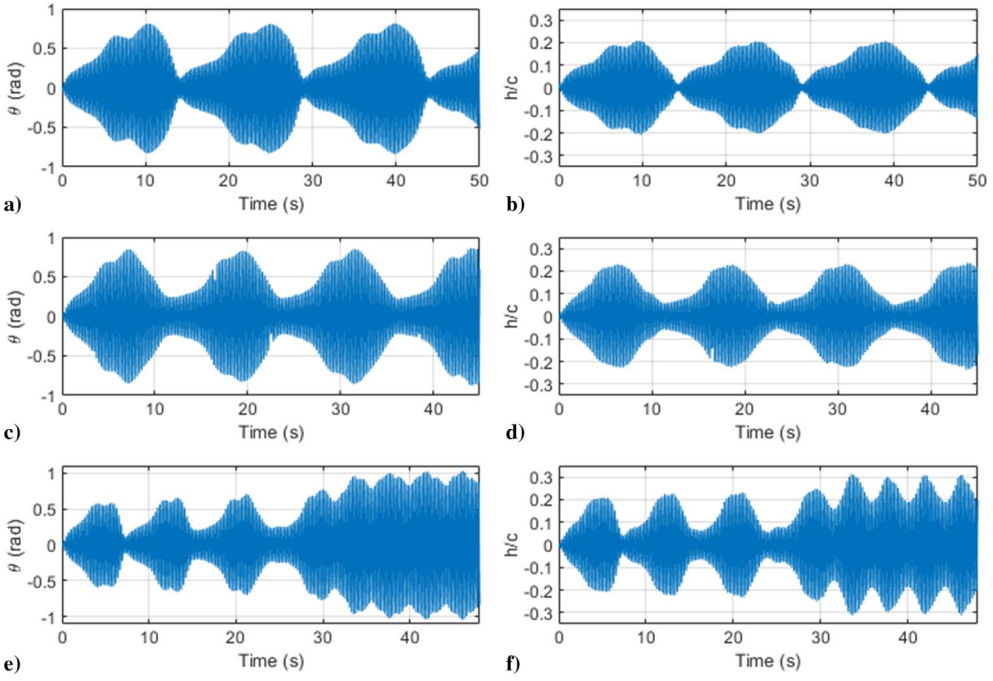

Fig. 10 Wing response showing growth-decay cycles at new dynamic pressures of a,b) 52.7 Pa (1.10 lb/ft^2), c,d) 59.85 Pa (1.25 lb/ft^2), and e,f) 71.8 Pa (1.50 lb/ft^2), with pitch response in left column and heave response in right column.

$$C_L = \frac{2}{\rho U_\infty^2 c l_s}[m_{\text{total}}\ddot{h} + m_w b x_\theta \dot{\theta}^2 \sin(\theta) - m_w b x_\theta \ddot{\theta}\cos(\theta) + k_h h + c_h \dot{h} + F_f \text{sign}(\dot{h})] \tag{1}$$

$$C_M = \frac{2}{\rho U_\infty^2 c^2 l_s}[I_\theta \ddot{\theta} - m_w b x_\theta \cos(\theta)\ddot{h} + k_\theta(\theta)\theta + c_\theta \dot{\theta} + M_f \text{sign}(\dot{\theta})] \tag{2}$$

and used to calculate the instantaneous power into and out of the wing as a result of the aerodynamic lift and moment, as seen in Eq. (3):

$$P_L = C_L \frac{1}{2}\rho U_\infty^2 c l_s \dot{h}, \quad P_M = C_M \frac{1}{2}\rho U_\infty^2 c^2 l_s \dot{\theta} \tag{3}$$

Additionally, the coupling energy, which describes the flow of energy from one degree of freedom into another, can be found by integrating the product of the mass coupling terms and the pitch and heave derivatives over the course of a single oscillation, as shown in Eq. (4):

$$E_{x_\theta,h} = \int_0^T (m_w b x_\theta \ddot{\theta}\cos\theta - m_w b x_\theta \dot{\theta}^2 \sin(\theta))\dot{h}\,\mathrm{d}t,$$
$$E_{x_\theta,\theta} = \int_0^T m_w b x_\theta \ddot{h}\cos(\theta)\dot{\theta}\,\mathrm{d}t \tag{4}$$

Table 4 Comparison of upper and lower bounds for equivalent third region of interest (characterized by growth-decay cycles) at differing freestream dynamic pressures in terms of f_{osc}/f_{LCO}

Prescribed freestream dynamic pressure	Average inherent LCO frequency, Hz	Region 3 VFDG frequency lower bound (f_{osc}/f_{LCO})	Region 3 VFDG frequency upper bound (f_{osc}/f_{LCO})
47.9 Pa (1.00 lb/ft^2)	4.05	0.975	0.998
52.7 Pa (1.10 lb/ft^2)	3.94	0.974	0.984
59.85 Pa (1.25 lb/ft^2)	3.95	0.951	0.969
71.8 Pa (1.50 lb/ft^2)	3.94	0.939	0.954

Positive values for $E_{x_\theta,h}$ denote energy moving from the pitch degree of freedom into the heave degree of freedom, whereas positive values for $E_{x_\theta,\theta}$ denote energy from the heave degree of freedom into the pitch degree of freedom. The aeroelastic wing apparatus used in this work was identical to the system used by Kirschmeier et al. [25]; therefore, the system identification performed by Kirschmeier et al. [25] is applied here. Kirschmeier et al. [25] examined the average power and energy on a cycle-to-cycle basis of the individual oscillations in pitch and heave. However, in this work, because the amplitudes of the pitch and heave oscillations are constantly changing, the time history of the power and coupling energy will be observed for the extent in which the disturbance generator vortices are interacting with the aeroelastic wing. This will highlight the changes in these parameters as the wing behavior changes, especially when it is experiencing amplitude growth-decay cycles.

The aerodynamic powers due to the lift and pitching moment, shown in Figs. 11 and 12, vary considerably between the five regions of interest discussed in Sec. III.C and summarized in Table 3. When power is positive, it signifies energy moving from the flow into the aeroelastic wing; and when negative, the reverse is true. Tests in regions 1 and 5 characterized by small-amplitude buffeting exhibit strictly positive power due to lift, whereas those in regions 2 through 4 and exhibiting LCOs or growth-decay cycles show fluctuating power due to lift, with both positive and negative portions within each oscillation cycle. For all five regions of interest, power due to the aerodynamic moment contains both negative and positive portions within each oscillation cycle. Peak power in cases from the third region of interest occurs just before the peak pitching amplitude, whereas the minimum absolute value of the power occurs as the wing pitch and heave approach their minimums, as seen in Figs. 11c and 12c. In the case when the disturbance generator frequency is approximately equal to the LCO frequency (region 4), the power from both the lift and aerodynamic moment mimics the behavior of the wing motion, exhibiting an initial spike before leveling off to a constant amplitude. However, the maximum negative power is not equivalent to the maximum positive power, implying that more energy is fed into the aeroelastic system than is released back into the flow in all cases. This is consistent with the expected results in consideration of friction losses throughout the system. Additionally, maximum power due to lift is higher than power due to the aerodynamic moment in all regions of interest except for region five. For tests in this region, the power due to aerodynamic moment is great than the power due to lift.

The coupling energy between the pitching and heaving degrees of freedom, shown in Fig. 13, generally mimics the envelope of the wing pitch oscillations. Following the convention discussed for Eq. (4), the

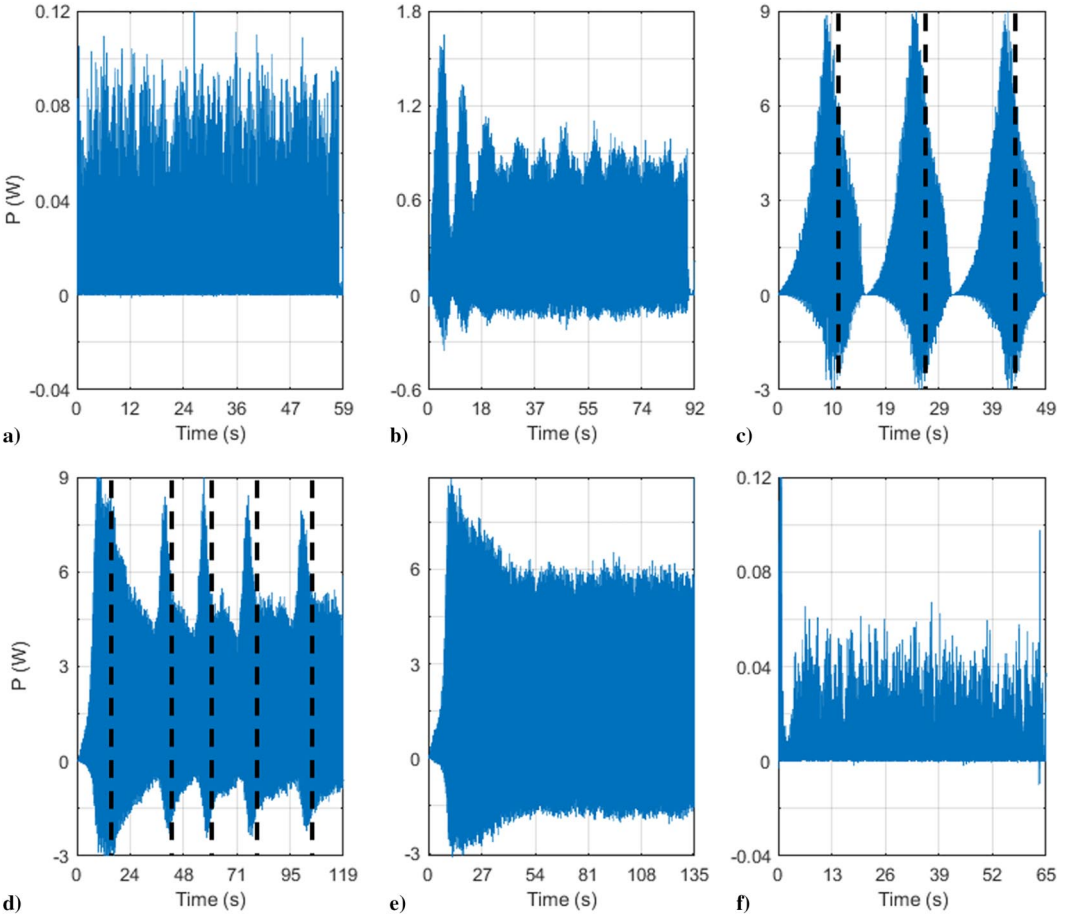

Fig. 11 Power due to lift for disturbance generator oscillation frequencies of a) 3.5 Hz, b) 3.93 Hz, c) 4.00 Hz, d) 4.04 Hz, e) 4.05 Hz, and f) 4.50 Hz, representing five regions of interest for test cases at 47.9 Pa (1.00 lb/ft^2), with two tests from third region (Figs. 11c and 11d). Vertical lines represent amplitude peaks in heave DOFs.

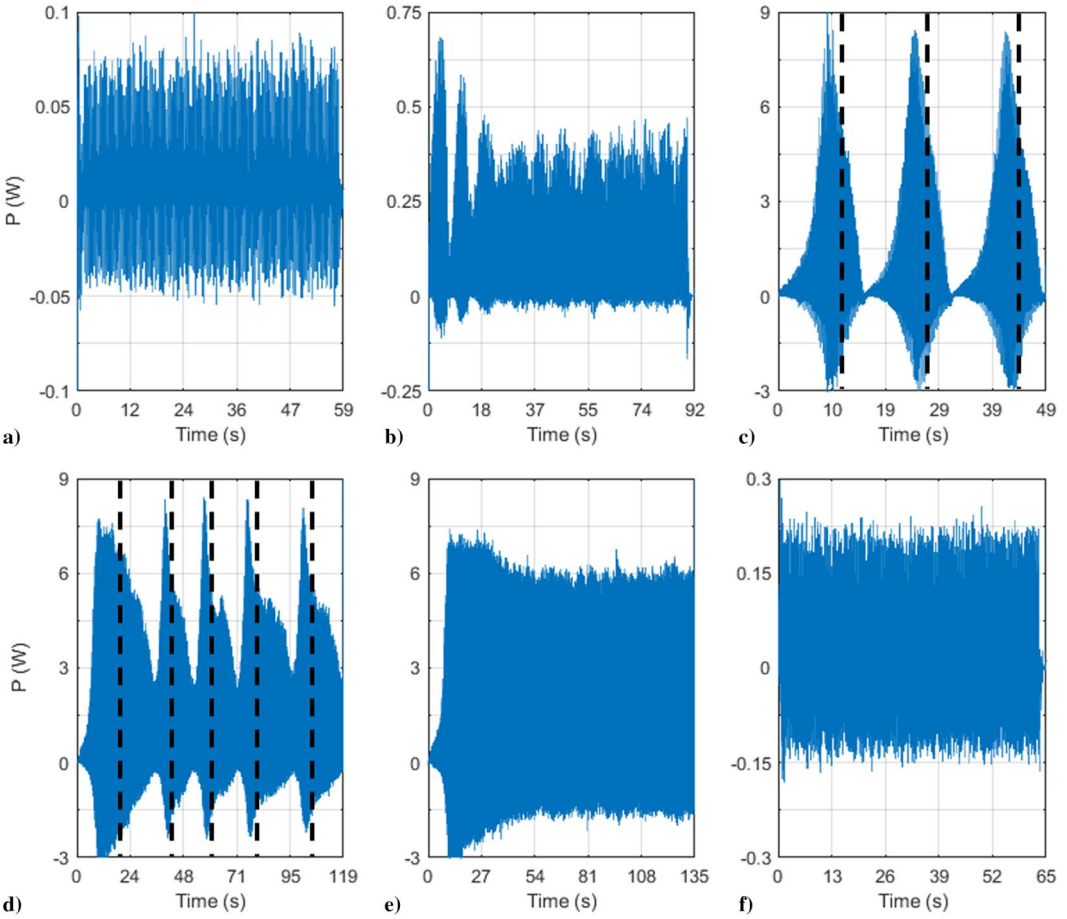

Fig. 12 Power due to aerodynamic moment for disturbance generator oscillation frequencies of a) 3.5 Hz, b) 3.93 Hz, c) 4.00 Hz, d) 4.04 Hz, e) 4.05 Hz, and f) 4.50 Hz, representing five regions of interest for test cases at 47.9 Pa (1.00 lb/ft^2), with two tests from third region (Figs. 12c and 12d). Vertical lines represent amplitude peaks in pitch DOFs.

results show that for cases in regions 1 through 4, with disturbance generator frequencies from 3.5 to 4.05 Hz, $E_{x_\theta,\theta}$ is always positive while $E_{x_\theta,h}$ is always negative, indicating the flow of energy is strictly from the heave DOF into the pitch DOF. Only when the disturbance generator frequency passes the inherent LCO frequency (region 5) does the flow of energy change directions. This change may be one of the underlying causes for the wing response asymmetry about the LCO frequency.

B. Comparison to Classical Wave Interference

For the third region of interest, discussed in Sec. III.C, the wing experienced periodic amplitude growth and decay in the presence of incoming flow disturbances near the inherent LCO frequency. Because the disturbance generator oscillations are prescribed as sinusoids and the wing pitch and heave display sinusoidal motion, signal processing techniques can be employed to compare the wing dynamics to classical wave interference in an effort to understand the underlying causes of this behavior. A simple model using the assumption of classical wave interference of the form $g(t) = A\sin(2\pi f_1 t) + A\sin(2\pi f_2 t)$ was constructed using a baseline sinusoidal signal with a prescribed frequency of 4.05 Hz, matching the experimental results from undisturbed tests at 47.9 Pa (1.00 lb/ft^2). The second sine wave, with equivalent magnitude and a frequency ranging from 3.95 to 4.04 Hz, was used to represent the effects of the incoming vortices produced by the disturbance generator for test cases at 47.9 Pa (1.00 lb/ft^2). The resulting combined signal, shown in Fig. 14a, shows the familiar beat pattern of two sinusoids with similar frequencies.

Comparing the wing response in the wake of the disturbance generator to classical wave interference, the envelopes of both pitching and heaving oscillations have similar shapes to the resultant wave from two sinusoids with similar frequencies, as seen in Fig. 14. In both instances, the profile is marked by periodic growth and decay cycles with a considerable difference in magnitude between the maximum and minimum values. In the classical wave interference assumption, the growth-decay cycle is symmetric in time about the peak amplitude; but, in the empirical data, this is not always the case. For test cases at 47.9 Pa (1.00 lb/ft^2), when the disturbance generator oscillation frequency is set to 3.95 Hz, the growth period in both pitch and heave degrees of freedom is longer than the decay period; whereas at 4.03 Hz, the decay period is longer than the growth period, as shown in Fig. 15. In addition to the similarities between the signal envelopes, the growth-decay cycle period, which is equivalent to the beat frequency in classical wave interference, is similar between the classical wave interference assumption and the empirical data for cases from 3.95 to 3.99 Hz but begins to deviate as the disturbance generator frequency approaches the LCO frequency. As the disturbance generator frequency approaches 4.05 Hz, the growth-decay cycle period does not increase at the same rate as it would in classical wave interference, as shown in Fig. 16.

Although there are similarities between classical wave interference and the interaction of the aeroelastic wing with the incoming flow disturbances, there are a number of differences that highlight the complexities of the nonlinear nature of aeroelastic system. In classical wave interference, the instantaneous phase between the two signals in question changes, but at a constant rate. The same is also true of the phase difference between the combined signal and either one of the original signals. In the case of the aeroelastic system in this work, the phase difference between the disturbance generator oscillations and either the pitch or heave, analogous to the combined signal, changes at a variable rate. For cases with disturbance generator frequencies from 3.95 to 4.03 Hz and freestream dynamic pressure of 47.9 Pa (1.00 lb/ft^2), the rate of change of this phase difference is near zero when the amplitude of the pitch or heave is at its minimum during the cycle and peaks just before the amplitude maximum, as shown in Fig. 17. In addition to

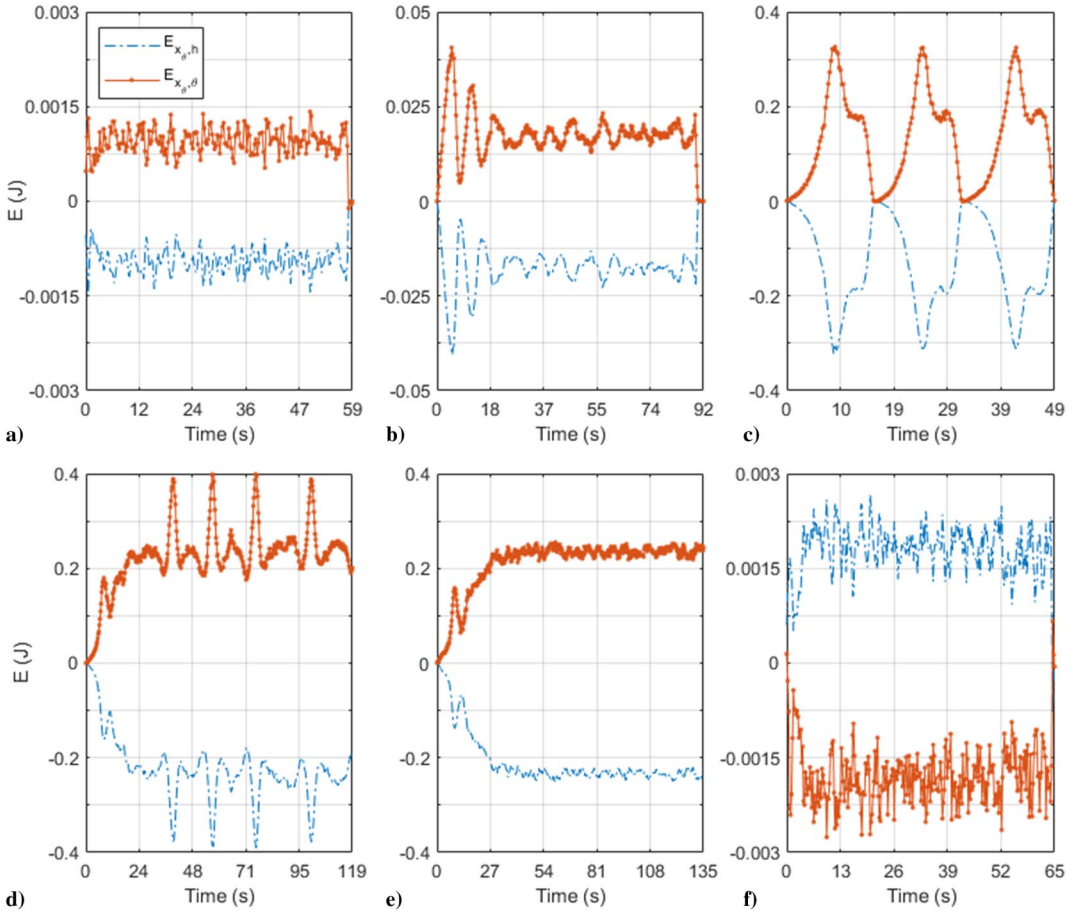

Fig. 13 Coupling energy between pitch and heave degrees of freedom for disturbance generator oscillation frequencies of a) 3.5 Hz, b) 3.93 Hz, c) 4.00 Hz, d) 4.04 Hz, e) 4.05 Hz, and f) 4.50 Hz, representing five regions of interest for test cases at 47.9 Pa (1.00 lb/ft^2), with two tests from third region (Figs. 13c and 13d).

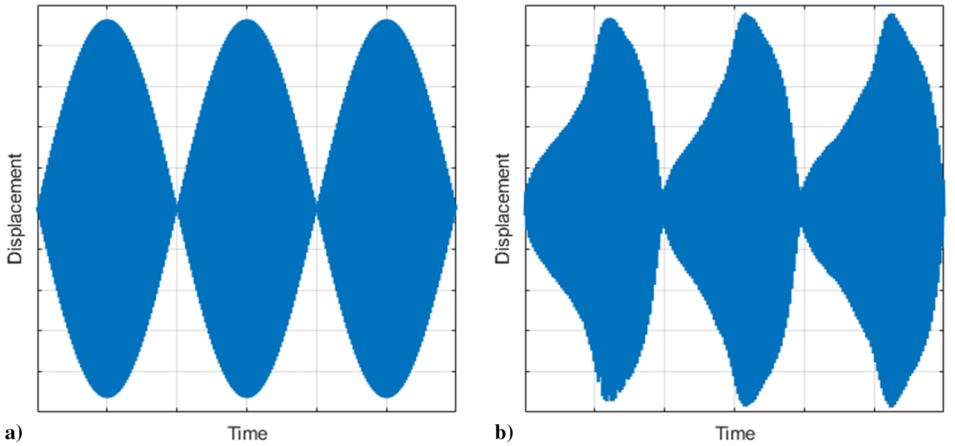

Fig. 14 Comparison between a) classical wave interference using sine waves with frequencies of 4.00 and 4.05 Hz and b) wing pitch angle when disturbance generator oscillation frequency is set to 4.00 Hz and freestream dynamic pressure is set to 47.9 Pa (1.00 lb/ft^2).

the differing phase behavior, classical wave interference is independent of whether the frequency of the interfering signal is greater than or less than the original signal. However, in the case of the aeroelastic wing, once the disturbance generator frequency passes beyond the LCO frequency, the wing response drastically changes and is completely absent of the growth-decay cycles, as discussed in Sec. III.C and shown in Fig. 7.

C. Frequency Analysis of Pitch and Heave Oscillations

Unsurprisingly, attempting to model the nonlinear behavior of the aeroelastic wing using classical wave interference falls short in capturing the full picture. Analyzing the frequency content of the wing response as it interacts with the incoming flow disturbances provides insight on whether the wing behavior is the result of only a few interacting sinusoidal oscillations or if the nonlinearities inherent in aeroelastic systems create more complexity.

The frequency content of the pitch and heave oscillations were analyzed using MATLAB's fast-Fourier transform function with 1×10^6 padding zeros and a Chebyshev windowing technique applied to the data to improve frequency resolution. For test cases at 47.9 Pa (1.00 lb/ft^2), the first, second, and fifth regions of interest show that the dominant frequencies of the pitch and heave

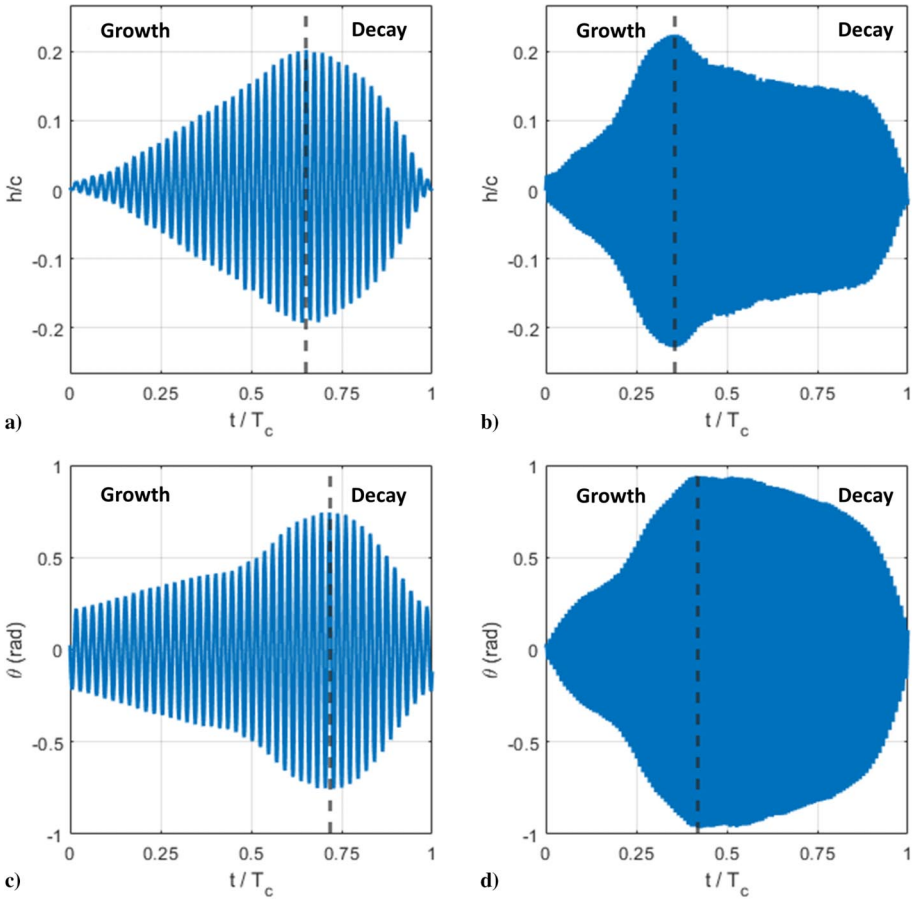

Fig. 15 Comparison between growth period and decay period over one cycle for a) heave at 3.95 Hz and b) 4.03 Hz; and pitch at c) 3.95 Hz and d) 4.03 Hz, for test cases at 47.9 Pa (1.00 lb/ft^2).

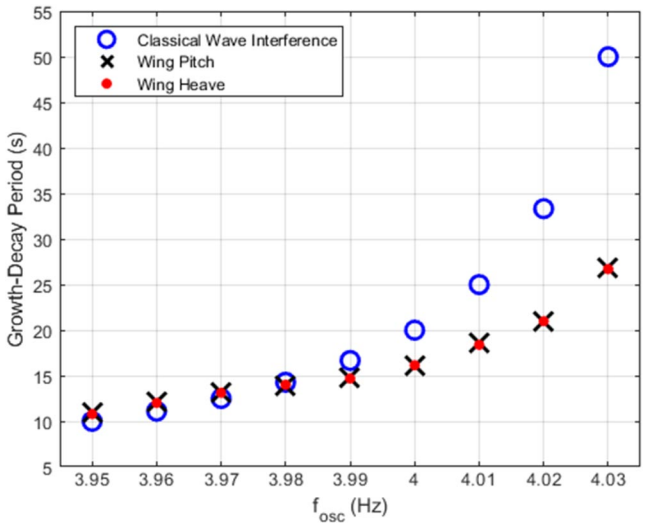

Fig. 16 Comparison of growth-decay cycle period between classical wave interference and pitch and heave oscillations in aeroelastic wing for test cases at 47.9 Pa (1.00 lb/ft^2).

oscillations are equal to the disturbance generator oscillation frequency. However, in the third region of interest, the dominant frequencies of both pitch and heave oscillations show a large jump, with the dominant frequency being equivalent to the LCO frequency seen in the undisturbed test at the same dynamic pressure. Compared to the undisturbed tests, which showed a single dominant frequency in both pitch and heave degrees of freedom, the resulting frequency spectrum for the cases from 3.95 to 4.03 Hz showed multiple dominant frequencies. Although the largest frequency peak in these cases corresponds to the wing LCO frequency, as shown in Figs. 18a and 18b, the disturbance generator frequency is also clearly visible, usually as the second largest peak. Several additional peaks are also present, decreasing in magnitude as their distance from the LCO frequency increases. If the resulting pitch or heave motion was based purely on the interference of two signals (one representing the disturbance generator oscillation and the other representing the inherent LCO behavior), the resulting FFT would show only two dominant peaks, as seen in Fig. 18c. When the disturbance generator frequency was set to 4.05 Hz, a single dominant frequency was again present, representing both the LCO frequency and the disturbance generator frequency. A full summary of the FFT results can be seen in Fig. 19.

D. Comparison to Existing Studies and Potential Applications

Contrasting with the previous work done in this research group by Kirschmeier et al. [22], which saw spontaneous LCO annihilation as a result of vortices produced by a static bluff body at frequencies near three times f_{LCO}, this spontaneous annihilation was not seen during any of the test cases performed using the VFDG. However, the presence of the periodic growth-decay cycles when approaching the LCO frequency presents a unique opportunity when coupled with the disturbance generator's active control, allowing for on-demand starting or stopping of its oscillations. If the wing is initially at rest, the disturbance generator can be used to excite LCOs as the impinging vortices push the aeroelastic wing above the required pitch amplitude needed to begin LCOs. If the disturbance generator oscillations are stopped as the wing approaches the peak amplitude in pitch, the wing will transition to self-sustaining LCOs, as shown in Fig. 20. Conversely, the disturbance generator can also be used to annihilate existing LCOs by first inducing the periodic growth-decay cycles and then stopping oscillations as the wing nears minimum amplitude in pitch and heave, as shown in Fig. 21. For test cases at 47.9 Pa

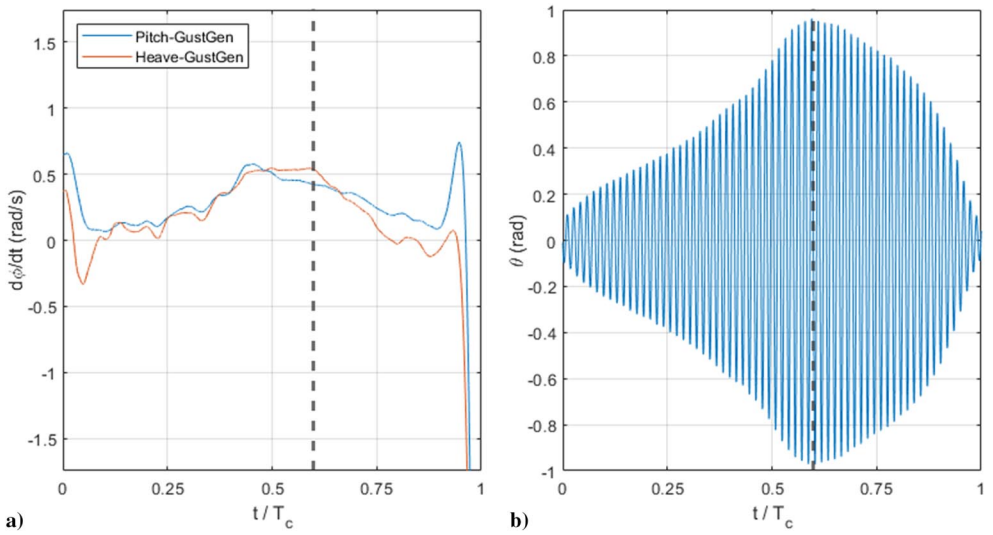

Fig. 17 Relationship between a) rate of change of phase difference between disturbance generator oscillations and wing pitch and heave, and corresponding b) wing pitch amplitude over course of a single growth-decay cycle. Dashed lines mark peak pitching amplitudes in both plots.

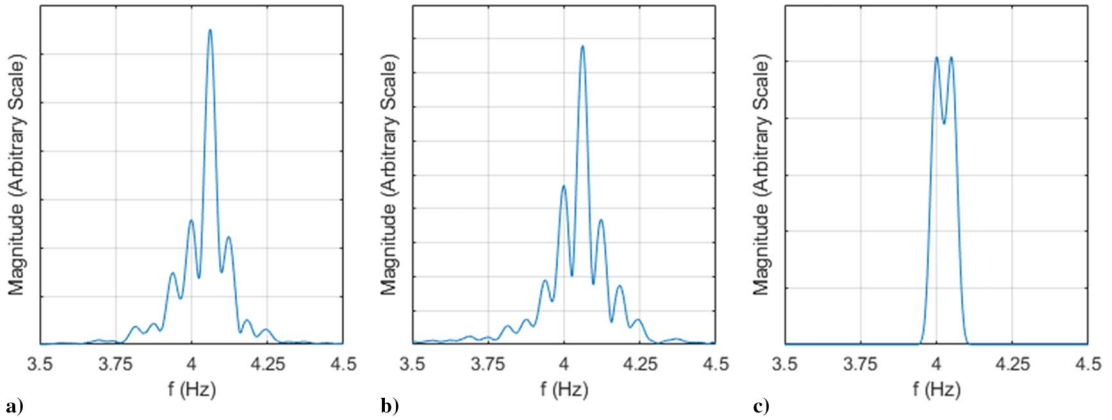

Fig. 18 FFTs of a) pitch oscillations and b) heave oscillations for a test case at freestream dynamic pressure of 47.9 Pa (1.00 $\mathrm{lb/ft^2}$), with disturbance generator oscillation frequency set to 4.00 Hz clearly showing multiple dominant frequencies; and c) classical wave interference assumption showing frequency spikes at only two input sine waves.

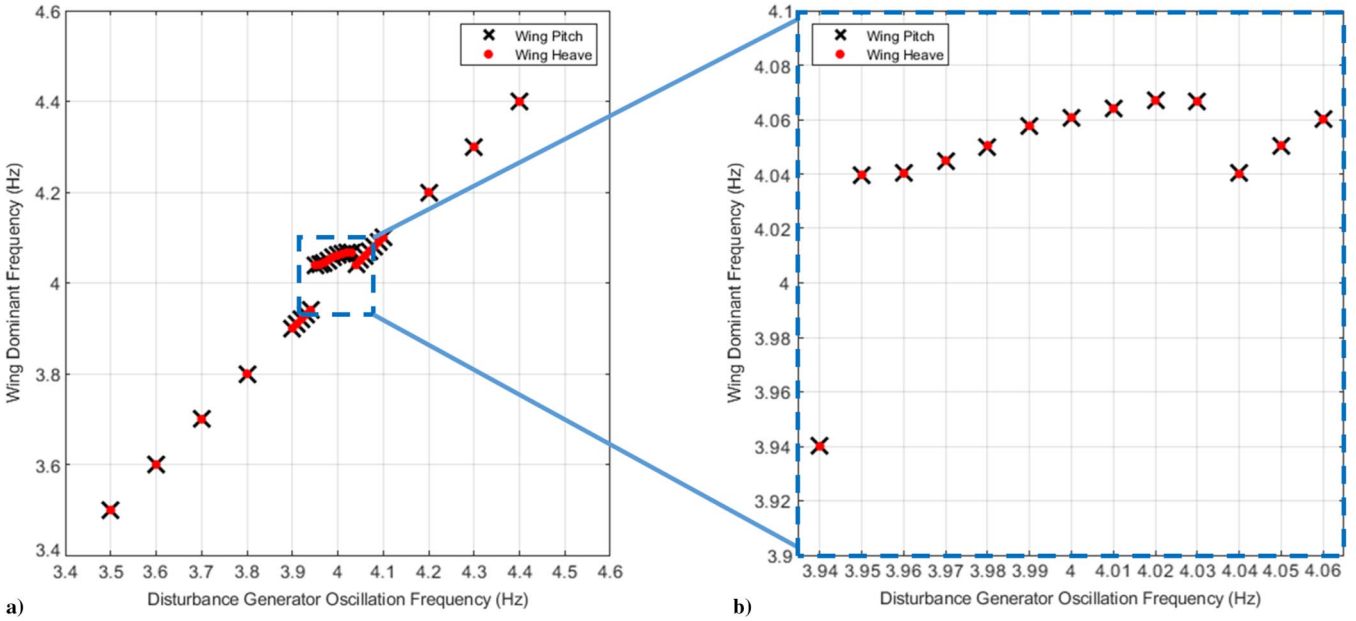

Fig. 19 Wing dominant frequency responses for test cases at 47.9 Pa (1.00 $\mathrm{lb/ft^2}$) as a function of disturbance generator oscillation frequency for a) all oscillation frequencies and b) oscillation frequencies from 3.94 to 4.06 Hz.

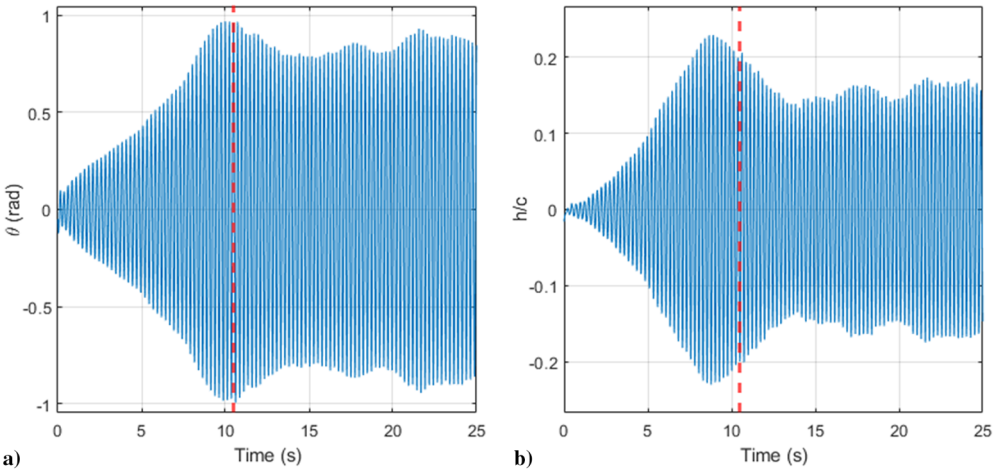

Fig. 20 LCO excitation using variable-frequency disturbance generator oscillating at 4.00 Hz, showing a) pitch and b) heave transition to self-sustaining LCOs. Red lines mark times when disturbance generator oscillations were stopped.

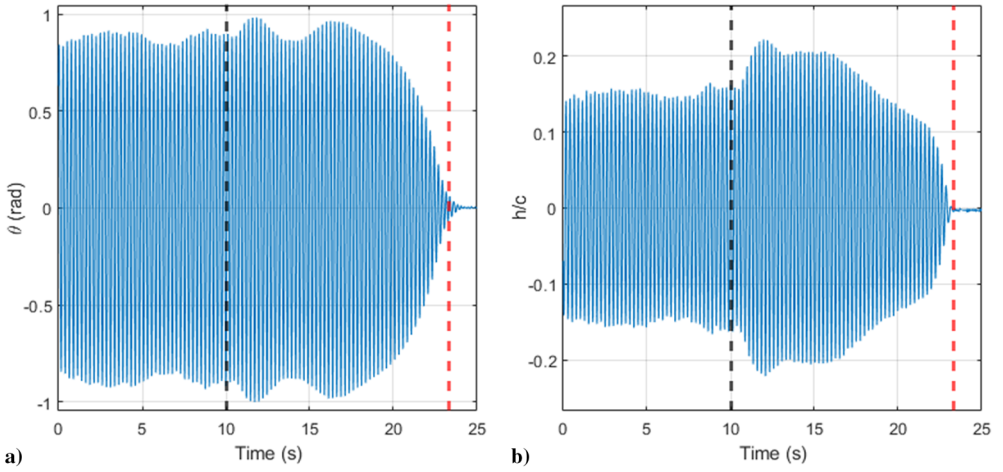

Fig. 21 LCO annihilation using variable-frequency disturbance generator oscillating at 4.00 Hz, showing a) pitch and b) heave. Black lines signify when disturbance generator oscillations started, whereas red lines show when oscillations stopped.

(1.00 lb/ft^2) with disturbance generator frequencies ranging from 3.95 to 4.04 Hz, LCO excitation and annihilation were achieved. At 4.05 Hz, which is approximately equal to the LCO frequency, the wing entered LCOs as a result of vortices produced by the disturbance generator but did not display the periodic growth-decay cycles present in tests at lower frequencies. Rather, the wing continued to oscillate at a constant amplitude above 55 deg. As a result, annihilation was not achieved and the LCOs were stopped by decreasing the dynamic pressure in the wind-tunnel test section. Below 3.95 Hz, the maximum pitching amplitude fell below the required threshold to excite the wing. Above 4.05 Hz, the wing response was marked by an initial spike in amplitude, but which did not bring it above the threshold needed to excite LCOs. For the additional dynamic pressures of 52.7 Pa (1.10 lb/ft^2) and 59.85 Pa (1.25 lb/ft^2), LCO excitation and annihilation were achieved using the same method. However, while the tests run at higher dynamic pressures displayed behavior indicative of region 3, that is the amplitude growth-decay cycles, tests run at 71.8 Pa (1.50 lb/ft^2) were only able to excite LCO. Annihilation was not observed due to the secondary growth-decay cycle behavior discussed in Sec. III.D, which displayed higher minimum amplitudes within the growth-decay cycles.

The work done by Okshai et al. [20] (discussed in Sec. I) contained similarities in the experimental setup as compared to this work. However, the airfoil used in their study was configured quite differently. Both studies showed amplitude modulation in the presence of the incoming flow disturbances and a high degree of sensitivity to the frequency of the disturbances. This may suggest that aeroelastic systems displaying LCOs that are subjected to incoming flow disturbance may be controlled by tailoring the amplitude and frequency of such disturbances. A control device with appropriate design could produce flow disturbances at a wide range of frequencies and amplitudes to produce a desired result in a downstream aeroelastic system including LCO excitation and amplitude enhancement or LCO annihilation.

V. Future Work

Future work may include developing a control framework that could use the wing sensors (pitch angle and heave displacement) in conjunction with the active disturbance generator control to sense when the wing enters LCOs and use the disturbance generator to annihilate the LCOs without the need for human input. The control scheme could make use of state machine architecture to determine the LCO state of the wing and then trigger a feedback control loop to provide active input for the disturbance generator oscillation amplitude and frequency. Additionally, parameters of the aeroelastic system, such as spring stiffness and center of mass location, could be studied to determine the sensitivity of the system to the VFDG and understand its ability to be applied to a wide range of aeroelastic systems.

VI. Conclusions

This paper reported the design and implementation of a variable-frequency disturbance generator used to study the interaction between an aeroelastic wing and incoming flow disturbances. The experimental results were postprocessed and studied by observing

the wing pitch and heave time histories, applying an aeroelastic inverse method, and performing frequency analysis. The results of this study can be summarized by the following points:

1) The pitch and heave response of the aeroelastic wing in the presence of incoming flow disturbances was observed to be highly dependent on the oscillation frequency of the VFDG.

2) At VFDG oscillation frequencies approaching the inherent LCO frequency from below, the wing displayed cyclic amplitude growth and decay in both pitch and heave degrees of freedom.

3) Analysis of the coupling energy showed that below the inherent LCO frequency, energy flows from the heave degree of freedom into pitch degree of freedom. Above the inherent LCO frequency, the flow of energy is reversed, moving from the pitch degree of freedom into the heave degree of freedom.

4) Frequency and phase analysis of the wing motion showed that the system is more complex than a combination of two sinusoidal oscillations displaying classical wave interference but that it does have similarities that contribute to the growth-decay cycles present in test cases just below the inherent LCO frequency.

5) The VFDG was shown to be capable of both exciting LCOs and annihilating preexisting LCOs in the aeroelastic wing by approaching, but not matching, the inherent LCO frequency of the system.

Acknowledgments

Funding for this research provided by the National Science Foundation, and the authors are grateful for its financial support of this study under award no. CMMI-2015983, which is managed by Eva Kanso. Additional funding was provided by the U.S. Air Force Office of Scientific Research under award no. FA9550-17-1-0301, which is managed by Gregg Abate. The authors would like to thank Shreyas Narispur and Mingtai Chen for their guidance and training on operation of the North Carolina State University subsonic wind tunnel. Arun Vishnu Suresh Babu, Mariah Mook, and Daniel Hall were instrumental in assisting with the experimental campaign. Undergraduate Students Zachary Boulton and Ashwin Sivayogan were key in their work on the LabVIEW analysis code, which was used to record data during testing.

References

[1] Ricketts, R. H., "Experimental Aeroelasticity History, Status and Future in Brief," NASA TM-102651, April 1990.

[2] Garrick, I. E., and Reed, W. H., "Historical Development of Aircraft Flutter," *Journal of Aircraft*, Vol. 18, No. 11, 1981, pp. 897–912. https://doi.org/10.2514/3.57579

[3] Theodorsen, T., "General Theory of Aerodynamic Instability and the Mechanism of Flutter," NACA TR 496, 1935.

[4] Bryant, M., and Garcia, E., "Modeling and Testing of a Novel Aeroelastic Flutter Energy Harvester," *Journal of Vibration and Acoustics*, Vol. 133, No. 1, 2011, Paper 011010. https://doi.org/10.1115/1.4002788

[5] Abdelkefi, A., "Aeroelastic Energy Harvesting: A Review," *International Journal of Engineering Science*, Vol. 100, March 2016, pp. 112–135. https://doi.org/10.1016/j.ijengsci.2015.10.006

[6] Goodman, C., Hood, M., Reichenbach, E., and Yurkovich, R., "An Analysis of the F/A-18C/D Limit Cycle Oscillation Solution," *44th AIAA/ASME/ASCE/AHS/ASC Structures, Structural Dynamics, and Materials Conference*, AIAA Paper 2003-1424, 2003. https://doi.org/10.2514/6.2003-1424

[7] Hayes, W. B., and Sisk, K., "Prevention of External Store Limit Cycle Oscillations on the F/A-18E/F Super Hornet and EA-18G Growler Aircraft," North Atlantic Treaty Organization/Science and Technology Organization RTO-MP-AVT-152, Neuilly-Sur-Seine Cedex, France, 2008.

[8] Opgenoord, M. M. J., Drela, M., and Willcox, K. E., "Influence of Transonic Flutter on the Conceptual Design of Next-Generation Transport Aircraft," *AIAA Journal*, Vol. 57, No. 5, 2019, pp. 1973–1987. https://doi.org/10.2514/1.J057302

[9] Bichiou, Y., and Hajj, M. R., "Effectiveness of a Nonlinear Energy Sink in the Control of an Aeroelastic System," *Nonlinear Dynamics*, Vol. 86, No. 4, 2016, pp. 2161–2177. https://doi.org/10.1007/s11071-016-2922-y

[10] Pidaparthi, B., and Missoum, S., "Stochastic Optimization of Nonlinear Energy Sinks for the Mitigation of Limit Cycle Oscillations," *AIAA Journal*, Vol. 57, No. 5, 2019, pp. 2134–2144. https://doi.org/10.2514/1.J057897

[11] Strganac, T. W., Ko, J., Thompson, D. E., and Kurdila, A. J., "Identification and Control of Limit Cycle Oscillations in Aeroelastic Systems," *Journal of Guidance, Control, and Dynamics*, Vol. 23, No. 6, 2000, pp. 1127–1133. https://doi.org/10.2514/2.4664

[12] Ramesh, K., Murua, J., and Gopalarathnam, A., "Limit-Cycle Oscillations in Unsteady Flows Dominated by Intermittent Leading-Edge Vortex Shedding," *Journal of Fluids and Structures*, Vol. 55, May 2015, pp. 84–105. https://doi.org/10.1016/j.jfluidstructs.2015.02.005

[13] Poirel, D., Métivier, V., and Dumas, G., "Computational Aeroelastic Simulations of Self-Sustained Pitch Oscillations of a NACA0012 at Transitional Reynolds Numbers," *Journal of Fluids and Structures*, Vol. 27, No. 8, 2011, pp. 1262–1277. https://doi.org/10.1016/j.jfluidstructs.2011.05.009

[14] Sváček, P., Feistauer, M., and Horáček, J., "Numerical Simulation of Flow Induced Airfoil Vibrations with Large Amplitudes," *Journal of Fluids and Structures*, Vol. 23, No. 3, 2007, pp. 391–411. https://doi.org/10.1016/j.jfluidstructs.2006.10.005

[15] Bunton, R. W., and Denegri, C. M., "Limit Cycle Oscillation Characteristics of Fighter Aircraft," *Journal of Aircraft*, Vol. 37, No. 5, 2000, pp. 916–918. https://doi.org/10.2514/2.2690.

[16] Dowell, E., Edwards, J., and Strganac, T., "Nonlinear Aeroelasticity," *Journal of Aircraft*, Vol. 40, No. 5, 2003, pp. 857–874. https://doi.org/10.2514/2.6876.

[17] Lua, K. B., Lim, T. T., and Yeo, K. S., "Effect of Wing–Wake Interaction on Aerodynamic Force Generation on a 2D Flapping Wing," *Experiments in Fluids*, Vol. 51, No. 1, 2011, pp. 177–195. https://doi.org/10.1007/s00348-010-1032-8

[18] Lua, K. B., Zhang, X. H., Lim, T. T., and Yeo, K. S., "Effects of Pitching Phase Angle and Amplitude on a Two-Dimensional Flapping Wing in Hovering Mode," *Experiments in Fluids*, Vol. 56, No. 2, 2015, pp. 1–22. https://doi.org/10.1007/s00348-015-1907-9

[19] Kinsey, T., and Dumas, G., "Parametric Study of an Oscillating Airfoil in a Power-Extraction Regime," *AIAA Journal*, Vol. 46, No. 6, 2008, pp. 1318–1330. https://doi.org/10.2514/1.26253

[20] Oshkai, P., Iverson, D., Lee, W., and Dumas, G., "Reliability Study of a Fully-Passive Oscillating Foil Turbine Operating in a Periodically-Perturbed Inflow," *Journal of Fluids and Structures*, Vol. 113, Aug. 2022, Paper 103630. https://doi.org/10.1016/j.jfluidstructs.2022.103630

[21] Gianikos, Z. N., Kirschmeier, B. A., Gopalarathnam, A., and Bryant, M., "Limit Cycle Characterization of an Aeroelastic Wing in a Bluff Body Wake," *Journal of Fluids and Structures*, Vol. 95, May 2020, Paper 102986. https://doi.org/10.1016/j.jfluidstructs.2020.102986

[22] Kirschmeier, B. A., Gianikos, Z., Gopalarathnam, A., and Bryant, M., "Amplitude Annihilation in Wake-Influenced Aeroelastic Limit-Cycle Oscillations," *AIAA Journal*, Vol. 58, No. 9, 2020, pp. 4117–4127. https://doi.org/10.2514/1.J058942

[23] Rockwood, M., and Medina, A., "Controlled Generation of Periodic Vortical Gusts by the Rotational Oscillation of a Circular Cylinder and Attached Plate," *Experiments in Fluids*, Vol. 61, No. 2, 2020, pp. 1–13. https://doi.org/10.1007/s00348-020-2882-3

[24] Chatterjee, P., Jenkins, M., Babu, A. V. S., Medina, A., Gopalarathnam, A., and Bryant, M., "Tailored Bluff Body Motion for Generating Desired Wake Structures," AIAA Paper 2020-3007, 2020. https://doi.org/10.2514/6.2020-3007

[25] Kirschmeier, B., Pash, G., Gianikos, Z., Medina, A., Gopalarathnam, A., and Bryant, M., "Aeroelastic Inverse: Estimation of Aerodynamic Loads During Large Amplitude Limit Cycle Oscillations," *Journal of Fluids and Structures*, Vol. 98, Oct. 2020, Paper 103131. https://doi.org/10.1016/j.jfluidstructs.2020.103131

[26] Visbal, M. R., and Garmann, D. J., "Numerical Investigation of Spanwise End Effects on Dynamic Stall of a Pitching NACA 0012 Wing," AIAA Paper 2017-1481, 2017. https://doi.org/10.2514/6.2017-1481

[27] Hussain, A. K. M. F., and Reynolds, W. C., "The Mechanics of an Organized Wave in Turbulent Shear Flow. Part 2. Experimental Results," *Journal of Fluid Mechanics*, Vol. 54, No. 2, 1972, pp. 241–261. https://doi.org/10.1017/S0022112072000667

D. E. Raveh
Associate Editor